NRC Research Press

ARTICLE

Influence of joint strength variability in timber-frame structures: propagation of uncertainty through shear wall finite element models under seismic loading

C. Boudaud, J. Baroth, and L. Daudeville

Abstract: Results of tests performed on joints used in timber-frame construction allow characterizing the variability of their mechanical behavior, which differs substantially from one joint to the next. The parameters of a constitutive model of the joints and their variability are identified. Finite element (FE) models of a shear wall and a timber-frame house are used in nonlinear dynamic calculations to study the propagation of uncertainty through the structure. It demonstrates that for a single-story 6 m × 6 m house, the variations in mechanical strength of each connection do not significantly affect the structural behavior of the house. Both the numerical and experimental results (on a shaking table) are quite similar, proving the model accuracy, its ability to study the propagation of uncertainty and its relevance for future development (non-regular, multi-story buildings…). Moreover, a sensitivity analysis performed on a FE wall model under uncertain seismic loads reveals the importance of earthquake motion modeling.

Key words: timber joint resistance, variability, wood shear walls, probabilistic propagation of uncertainty, seismic loading.

Résumé : Cet article synthétise de nombreux résultats d'études expérimentales aux échelles d'assemblages, de murs, et de maison à ossature en bois. Le nombre important de résultats à l'échelle des assemblages permet de caractériser la variabilité de leur résistance. Un calage probabiliste d'une loi de comportement des assemblages est proposé. Une étude de propagation d'incertitudes à travers les modèles éléments finis de murs de contreventement est ensuite menée. L'influence de la variabilité matérielle est estimée à l'échelle structurale via des modèles 2D et 3D, qui sont confrontés à des résultats d'essais sur table vibrante de murs et d'une maison. L'influence de la variabilité matérielle se révèle faible. Ces résultats montrent que le modèle numérique reproduit de manière satisfaisante les résultats expérimentaux, qu'il permet de travailler sur la propagation d'incertitudes matérielles et qu'il propose une base solide pour le futur développement de modèles de structures plus complexes (irrégularité en plan, en élévation, bâtiments de plusieurs étages). Enfin, la variabilité du chargement sismique est évaluée en utilisant une méthode de génération d'accélérogrammes, les résultats à l'échelle du mur montrent qu'elle est non négligeable.

Mots-clés : résistance d'assemblages, variabilité, murs de contreventement, propagation d'incertitudes probabiliste, chargement sismique.

1. Introduction

Timber structures featuring metal connectors are fairly resistant under cyclic and seismic loadings thanks to joint ductility. The high energy dissipation due to the semi-rigid behavior of the joints is well known and documented in the literature, as modeled at either the scale of shear walls (Filiatrault 1990; White and Dolan, 1995; Shenton et al. 1997; Richard et al. 2002; Dujic and Zarnic 2004) or the scale of a building (Lam et al. 2002; Filiatrault et al. 2002).

This dissipation capacity however cannot be fully optimized when designing timber-frame structures due to constraints imposed by safety coefficients in design codes, mainly as a result of the brittle behavior of wood. Moreover, existing uncertainties with respect to geometry, materials, and loads could be better incorporated. Only a few studies have focused on the impact of mechanical behavior variability and seismic loading specific to timber-frame construction. Foliente (2000) limited his study to the impact of earthquake uncertainty. Yin and Li (2010) examined the effects of loading and strength uncertainties; however, their study was limited by "no data available for determining the probabilistic distribution of the hysteresis parameters". Moreover, the 10 parameters of the constitutive behavior law were all considered as random, thus restricting their evaluation to the scale of a shear wall, in assuming a uniform dispersion of collapse fragility over the entire building. Pei and Van de Lindt (2010) assessed the impact of construction quality, in considering for example that up to 20% of the sheathing-to-framing nails were missing. Since shear wall fabrication is now largely industrialized, this aspect has not been taken into consideration in the present paper (Rosowsky 2002).

Moreover, despite the experimental and numerical investigations conducted at the scale of a shear wall (Dinehard and Shenton 1998; Ceccotti and Karacabeyli, 2002; Boudreault et al. 2007) or building (Foliente 1997; Lam et al. 2002; Li and Ellingwood 2007; Pei et al. 2010), improvements are still required to better predict the seismic response of structures and better account for the influence of seismic loading in seeking reliability targets (Li and Ellingwood 2007, Riahi et al. 2013). In this context, the quantification of uncertainties has become a major issue and one that needs

Received 14 December 2015. Accepted 8 April 2016.

C. Boudaud. Groupe Ecole Supérieure du Bois, LIMBHA, Nantes, France.
J. Baroth and L. Daudeville. Univ. Grenoble Alpes, 3SR, F-38000 Grenoble, France; CNRS, 3SR, F-38000 Grenoble, France.
Corresponding author: C. Boudaud (email: clement.boudaud@ecoledubois.fr).

Fig. 1. Test specimens and testing apparatus.

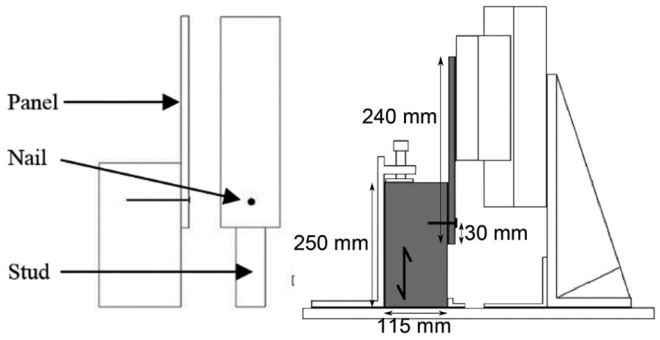

to be addressed to optimize the safety coefficients for achieving a targeted safety level.

To meet this objective, several tasks have been performed. First, a series of complementary experimental and numerical studies has yielded an adequate representation of the hysteretic behavior of timber-frame connections (Boudaud et al. 2014). This paper will present the subsequent step, which entails a synthesis of experimental data on joints along with the propagation of quantified variabilities on timber shear walls to analyze the corresponding influence on the response of timber structures under seismic loading.

Over 400 tests were performed on metal fasteners; these results have served to identify deterministic hysteretic constitutive models for three type of joints: sheathing-to-framing connections in shear walls, nail joints in roof truss assemblies, and 3D bracket-type connectors used to assemble roof trusses on the walls. The tests were repeated two or three times for monotonic loadings and five times for cyclic loadings. Many publications have dealt with sheathing-to-framing joint testing (He et al. 2001; Fulop et al. 2006; Xu and Dolan 2009; Germano et al. 2015; Sartori and Tomasi 2013; Verdret et al. 2015), but only Fonseca et al. (2002), working within the framework of the CUREE project, actually conducted a campaign on a very large number of specimens. The specimen testing protocol however was too dissimilar from current practices in Western Europe, which justifies the testing campaign presented herein.

This paper will first discuss the tests carried out on joints. The variability of the maximum bearing capacity of joints will be examined; this force will be applied to calibrate a versatile behavior law for joints with metal fasteners (Humbert et al. 2014). Next, the propagation of uncertainties at the joint scale will be analyzed through finite element (FE) models of walls and a 3D building (one-story house). This analysis will include a description of both the shear wall FE model (which has already been contrasted with results of tests performed on shear walls under quasi-static (14 tests) and dynamic (12 tests) loadings (Boudaud et al. 2014)) and the FE model of a house (a comparison with shaking table test results will also be provided in this paper). Lastly, the impact of seismic loading uncertainty will be investigated at the scale of a shear wall.

2. Strength variability of joints used in timber construction

This section will present a summary of results from tests performed on joints made with metal connectors. The variability in the mechanical behavior of these joints will be analyzed. The constitutive behavior law introduced to model these joints will be described, along with the relevant adaptation steps for taking into account the variability of mechanical behavior.

Table 1. Tested configurations of sheathing-to-framing nail joints.

Configuration	Nail size	Shape	Material	Panel type	Panel thickness (mm)
N1, N2, N3	2.1×45	RS	SS	OSB 3	9, 12, 15
N18, N19, N20	2.5×60	RS	SS	OSB 3	9, 12, 15
N25, N26, N27	3.1×85	RS	SS	OSB 3	9, 12, 15
N4, N5	2.1×45	RS	ZP	OSB 3	9, 12
N16, N17	2.5×50	RS	ZP	P 5	10, 16
N6, N7	2.1×55	RS	ZP	OSB 3	9, 15
N21, N22	2.8×80	RS	ZP	OSB 3	9, 15
N8, N9	2.3×60	RS	Ga	OSB 3	9, 15
N30, N31	3.1×90	RS	Ga	OSB 3	9, 15
N14, N15	2.3×60	X	SS	OSB 3	9, 15
N28, N29	3.1×85	X	SS	OSB 3	9, 15
N12, N13	2.3×60	X	Ga	OSB 3	9, 15
N23, N24	3.1×75	X	Ga	OSB 3	9, 15
N10, N11	2.3×60	RS	Ga	P 5	10, 16
N32, N33	3.1×90	RS	Ga	P 5	10, 16

Note: RS, ring-shank nail; X, "X"-shaped cross section nail; SS, stainless steel (X5 CrNiMo 18-10); ZP, zinc-plated c3+ (15 μm); Ga, hot-dip galvanization (50 μm); OSB3, Type 3 OSB panel; P5, Type 5 particleboard (OSB & P5, according to EN 12369-1).

Table 2. Coefficient of variation by configuration and type of loading.

Configuration	Monotonic	Cyclic
N1	14.5	13.5
N2	5.2	10.7
N3	28.0	10.9
N4	18.0	7.8
N5	2.5	5.0
N6	—	29.1
N7	11.9	18.2
N8	17.4	17.5
N9	23.5	13.2
N10	6.5	10.8
N11	5.9	10.9
N12	2.9	12.9
N13	23.6	18.1
N14	33.2	5.0
N15	9.6	3.4
N16	10.3	13.6
N17	7.8	9.4
N18	—	8.2
N19	3.2	10.0
N20	6.5	11.5
N21	22.4	16.5
N22	10.1	22.1
N23	28.0	15.5
N24	5.6	9.6
N25	—	18.7
N26	—	10.9
N27	13.9	16.0
N28	16.4	11.3
N29	10.7	3.5
N30	2.7	19.5
N31	5.8	5.0
N32	3.5	13.6
N33	3.7	9.0
Mean	12.2	12.5

2.1. Synthesis of experimental data

In this study, tests have been conducted on both the sheathing-to-framing nail connections (Boudaud et al. 2010) and 3D bracket-type connectors used to assemble roof trusses on the walls. One key point of this paper is the discussion of the variability in mechanical behavior of timber joints. Some of the experimental data presented below can already be found in the literature. Especially,

Fig. 2. Test set-up on nail joints: (*a*) configuration N1; and (*b*) configuration N2.

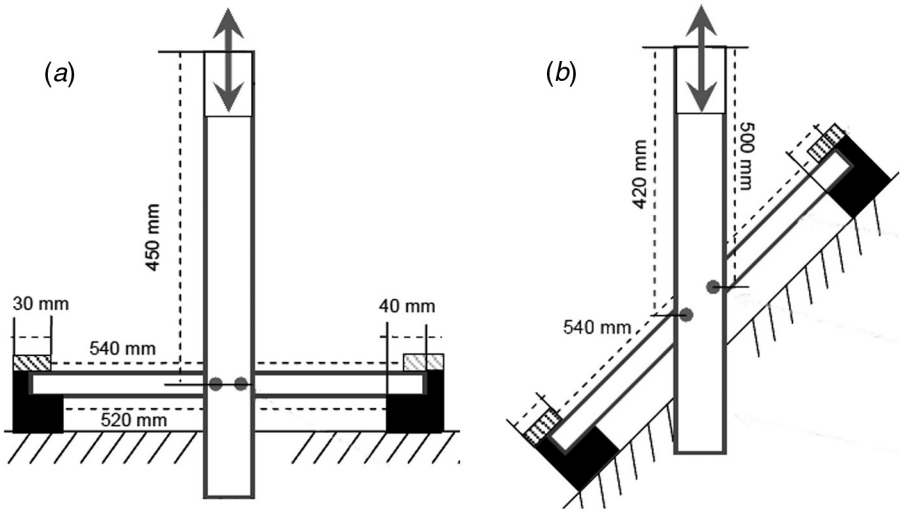

the average values of test results for sheathing-to-framing nail joints and for 3D bracket type connectors can be found in Appendix A of Humbert et al. (2014). However, these published results were not discussed and no information was given on their variability. The study of the third type of joints, roof truss / anti-buckling nail joints, is a totally unpublished work.

2.1.1. Sheathing-to-framing nail joints

A total of 33 nail joint configurations for sheathing were tested. The testing plan was based on the following variables: nail diameter (2.1, 2.3, 2.5, 2.8, and 3.1 mm), nail material (zinc-plated steel, hot-dip galvanized steel, and stainless steel), nail shape (ring-shank and X-shaped cross section), sheathing OSB panel thickness (9, 12, and 15 mm), and particleboard panel thickness (10 and 16 mm). Each configuration was tested under three monotonic and five cyclic loadings. Figure 1 shows the specimen and its installation in the testing machine. The test consisted of applying a shear force to the nail joint. Based on test results presented by Fonseca et al. (2002), both the grain orientation of the wood member and the panel orientation were considered to exert no influence. Table 1 details the 33 test configurations.

These results were processed by measuring the initial stiffness, maximum force, yield, and ultimate slips. Hereafter, only the variability in maximum force will be analyzed; the reason for this focus will be given in Section 2.3. For each joint configuration, the coefficient of variation (CV) of the corresponding maximum force will be calculated for the three monotonic tests and five cyclic tests. Results are listed in Table 2.

The average CV values are similar between monotonic and cyclic tests. Each CV has been calculated from a limited number of tests (either three or five); it may then be considered that an isolated value is irrelevant but the average of all values is indeed based on 165 tests (for cyclic loading).

2.1.2. Roof truss / anti-buckling nail joints

Two other nail joint configurations were also tested; they correspond to joints used to connect trusses top chords to beams connecting the trusses together and ensuring the horizontal stability perpendicular to the trusses. These joints are made with two nails: an N1 configuration with a 2.8 mm × 70-mm nail, and an N2 configuration with a 3.1 mm × 90-mm nail. Wood sections measure 35 mm × 100 mm. Figure 2*a* displays the specimen for the N1 configuration (with perpendicular timber members), while Fig. 2*b* reflects the N2 configuration (timber members at a 45° angle with one another). For each configuration, five monotonic and five cyclic tests were carried out.

Table 3. Coefficient of variation values of the maximum force for monotonic and cyclic testing and for configurations N1 and N2.

	Configuration	
Test	N1	N2
Monotonic	20.6	19.1
Cyclic	23.5	7.2

Table 3 provides the CV values of the maximum force under both monotonic and cyclic loadings. It should be pointed out that these values are quite high (up to 20%), except for cyclic loading under the N2 configuration (only 7.2%). No evidence is available to explain this observed difference, aside from the low number of results (five tests).

2.1.3. 3D bracket-type connectors

These connectors are used in shear walls and to connect roof trusses on the top plate of these walls. Tests were conducted in each direction, as indicated in Fig. 3. The wood member dimensions are 45 mm × 140 mm × 400 mm, and the specimens were fitted with 1, 2 or 4 brackets. The bracket type is a Simpson Strong-Tie® E5 (1.5 mm thick). Ring-shank nails (4 mm × 35 mm) were used to connect the brackets. Industrial trusses are generally connected to timber frame or masonry walls; hence, the brackets were either nailed to a wood member or bolted onto a metal plate. The test configurations are displayed in Table 4; for each one, three monotonic and five cyclic tests were carried out.

For each test, the maximum force was calculated, and the corresponding CV value is given in Table 5. As was the case for the sheathing nail joint, these CV values are similar under both monotonic and cyclic loadings. The mean CV of the maximum force under cyclic loading is averaged over 50 tests.

2.2. Constitutive behavior law

The constitutive law presented in Humbert et al. (2014) is able to model the mechanical behavior of joints made with metal connectors (nails, screws, staples, punched plates, 3D brackets, etc.). It is a versatile 1D analytical law that models pre-peak hardening and post-peak softening, hysteresis cycles and cumulative damage under a reverse loading. The model and its parameters have been fully detailed in the aforementioned paper. Of note, the parameters can be classified into 3 groups: (1) monotonic parameters describing the backbone curve under monotonic loading; (2) hysteretic

Fig. 3. 3D bracket-type connectors tested in each direction (respectively *X*, *Y*, and *Z*). [Colour online.]

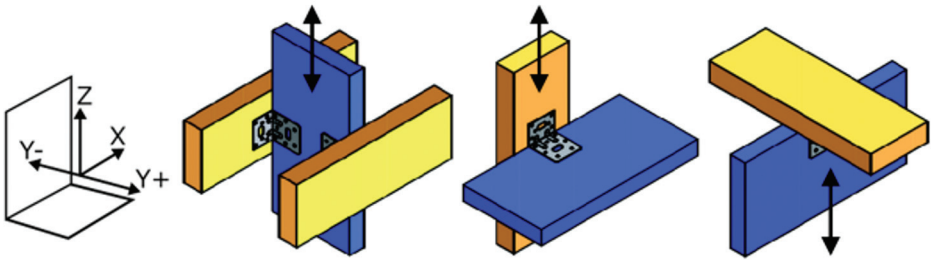

Table 4. Configurations of tested 3D bracket-type connectors.

Configuration	Direction	No. of brackets	Support
N1	X	4	Metal
N2			Timber
N3	Y	1	Metal
N4			Timber
N5		2	Metal
N6			Timber
N7	Z	2	Metal
N8			Timber

Table 5. Coefficient of variation values of the maximum forces of the tested bracket-type connectors, for configurations N1–N8.

	Test	
Configuration	Monotonic	Cyclic
N1	17.2	9.3
N2	9.1	4.3
N5	10.7	3.2
N6	4.5	13.7
N3	1.9	4.4
	31.6	12.7
N4	9.9	16.4
	11.1	16.3
N7	3.7	4.6
N8	1.4	14.0
Mean	10.1	9.9

parameters describing the shape of the hysteresis loops; and (3) damage parameters describing the cumulative damage of this joint.

The monotonic parameters introduced herein are quite similar to those proposed by Foschi (1974); they are calculated directly from the monotonic test. The other parameters are fitted to cyclic test results and require iterations over a few simulations. The fitting process has been described in depth in Humbert et al. (2014) and Boudaud et al. (2014), where it is shown how both the direct calibration (set of parameters for reproducing one particular test) and average calibration (set of parameters reproducing the average behavior over five tests) are obtained. Experience has shown that the parameters controlling the cyclic and damage behavior actually exhibit little variation for a given type of joint since the hysteretic loop shapes are relatively similar under such a loading.

2.3. Probabilistic calibration of the behavior law

One of the monotonic parameters in the constitutive law is the maximum force F_1. For each connector, F_1 proves to be the most influential factor (Humbert et al. 2009; Riahi et al. 2013). Under a cyclic displacement, the value of F_1 directly affects the entire backbone (envelope) curve and indirectly affects the damage model (maximum attainable force at a given displacement under reverse loading). For these reasons, only parameter F_1 will be used as a random parameter to model the variability of the mechanical behavior of metal joints. Based on this assumption, the result of such a calibration process will be presented below, with the N2 configuration (for 3D bracket-type connectors) being applied for illustration purposes in Fig. 4. In all, five cyclic tests were conducted on this configuration. From these results, the following steps have been implemented: (1) the envelope curve is calculated for each test; (2) the maximum force of each envelope curve is identified; (3) the mean and standard deviation of these curves are calculated; (4) on the hypothesis of a normal distribution of the F_1 parameter, the fractiles at 5% and 95% are calculated; (5) the cyclic behavior of the joint is simulated with F_1 set equal to $F_1^{5\%}$; and (6) this behavior is compared to the experimental envelope curves (monotonic responses) (Fig. 4*a*), and it is verified that the simulated cyclic behavior lies below the experimental curves.

The same set of steps are then performed for $F_1^{95\%}$ (Fig. 4*b*). Of note, Fig. 4 displays 10 envelope curves because the five envelope curves from the negative side (i.e., negative forces and displacements) are projected onto the positive side for greater clarity. These results tend to prove that using just the F_1 parameter as a random variable allows the model to replicate quite well the mechanical behavior variability of joints with metal connectors.

3. Propagation of uncertainty through finite element models (shear walls and a house)

The previous study on the mechanical variability of joints was aimed at conducting sensitivity analyses of timber structures under seismic loading. Both timber-frame walls and a full-scale one-story house will be studied in the following sections. These structures were subjected to shaking table tests. The FE model of the house was built according to a multi-scale approach (Boudaud et al. 2013). The sensitivity analysis therefore had to be carried out in two steps: first at the scale of a shear wall (using a refined 2D FE model), and second at the scale of an entire house thanks to a 3D FE model representing shear walls by 4-node macro elements. The shaking table tests will be briefly described in Section 3.1. All numerical developments presented in this paper were accomplished using the Code_Aster FE code, which is freely available under the GNU/GPL License (EDF 2014).

3.1. Shaking table tests

In the tests described below, the same ground motion has been applied to the shaking table at various amplitudes. The scenario for Guadeloupe (French West Indies) was selected (Boudaud et al. 2014). The most likely magnitude-distance couple was identified for this scenario with a return period of 475 years (i.e., a 10% probability of exceeding the peak ground acceleration in 50 years). The study was undertaken for ground type B (Eurocode 8 - CEN 2004). The resulting peak ground acceleration equaled 0.33g.

3.1.1. Shaking table tests on a single shear wall

The shear walls studied in this paper correspond to structural elements found in conventional timber-frame houses in Western

Fig. 4. Experimental envelope curves versus simulated behavior (N2 configuration for 3D bracket-type connectors): (*a*) 5% fractile of F_1; and (*b*) 95% fractile of F_1.

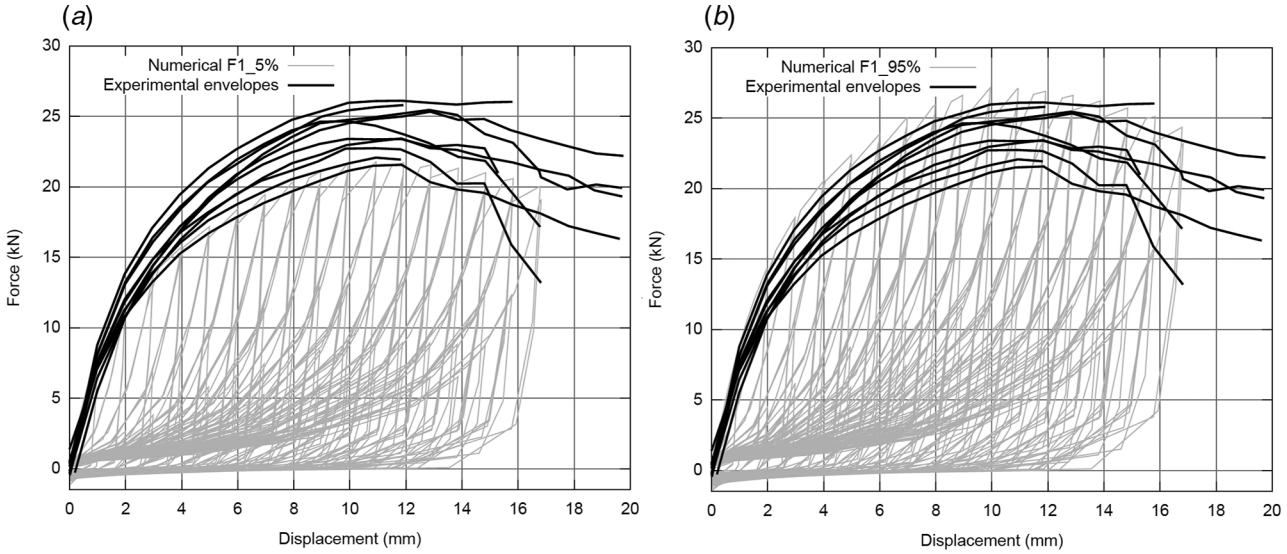

Fig. 5. Set-up for dynamic tests: (*a*) shear wall, FCBA, Bordeaux; and (*b*) house, CEA, Saclay. [Colour online.]

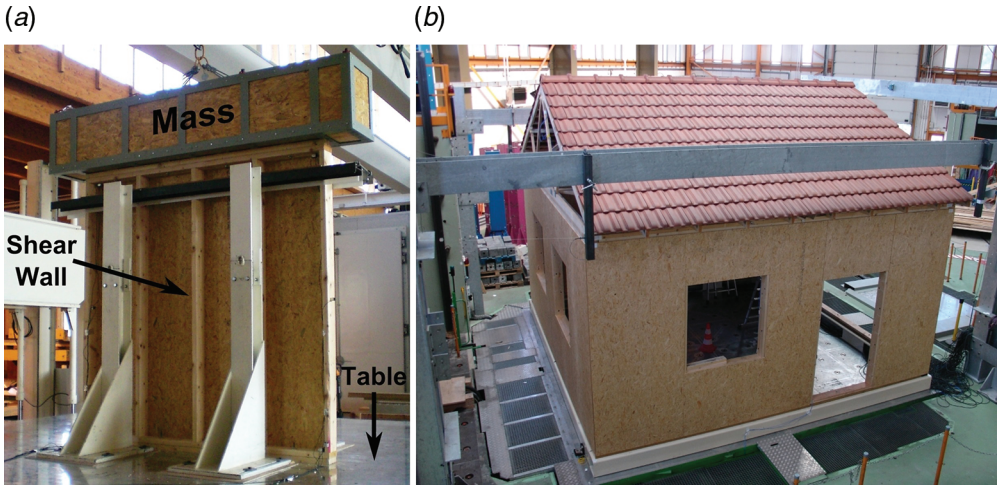

Europe. A full description of these walls is available in Humbert et al. (2014), and the dynamic tests are described in Boudaud et al. (2014). Figure 5*a* presents the set-up for testing a shear wall on the shaking table of the FCBA Technological Institute in Bordeaux, France. The shaking table with one translational degree of freedom (DOF) is able to reproduce the Guadeloupe accelerogram by relying on a lightweight structure (approx. max. 10 tons). The mass applied on top of the shear wall is intended to simulate the dead load due to the roof plus an upper story. Depending on the test, this mass was either 1500 or 2000 kg. The out-of-plane instability was limited by means of a frictionless guiding system. The shear wall sill plate was bolted to the table, and only reinforced 3D brackets were installed for exterior anchorage (AH2950/2, provided by Simpson Strong-Tie). These tests consisted of applying the Guadeloupe accelerogram (using direction (*Y*) providing the higher PGA) at a given peak ground acceleration (PGA) and then performing several tests with the same accelerogram and an increasing PGA. Each wall therefore was subjected to several loadings. The in-plane deformation of the wall was measured by means of a draw-wire sensor placed at the top of the wall, and an LVDT transducer allowed monitoring the shaking table displacement.

3.1.2. Shaking table tests on a house

Figure 5*b* presents a dynamic test performed on a single-story 6 m × 6 m timber-frame house. This testing campaign was conducted on the AZALEE 3D shaking table at the Tamaris facility in Saclay, France (Tamaris 2015). The Guadeloupe accelerogram was applied to each translational DOF of the shaking table. These tests were repeated with increasing PGA. Triaxial accelerometers and displacement sensors took measurements at 22 points on the structure (Charbonnel et al. 2014).

3.2. Propagation of uncertainty through the shear wall finite element models

Finite element modeling of shear walls is based on a beam, plate and two-node spring-like FE (Humbert et al. 2014). The constitutive behavior law presented above was implemented into the Code_Aster software. Euler beam elements serve to model the frame, while four-node DKT plate elements model the panels. Each two-node spring-like element models a metal fastener joint, whose properties were previously identified thanks to the calibration steps presented above. The resulting mesh is composed of 108 Panel-to-Frame (P2F), 8 Frame-to-Frame (F2F nail), and 2 F2F (angle) spring-like elements. The F2F joints exhibit different behavior

Fig. 6. FE model of the house: location and name of the displacement sensors.

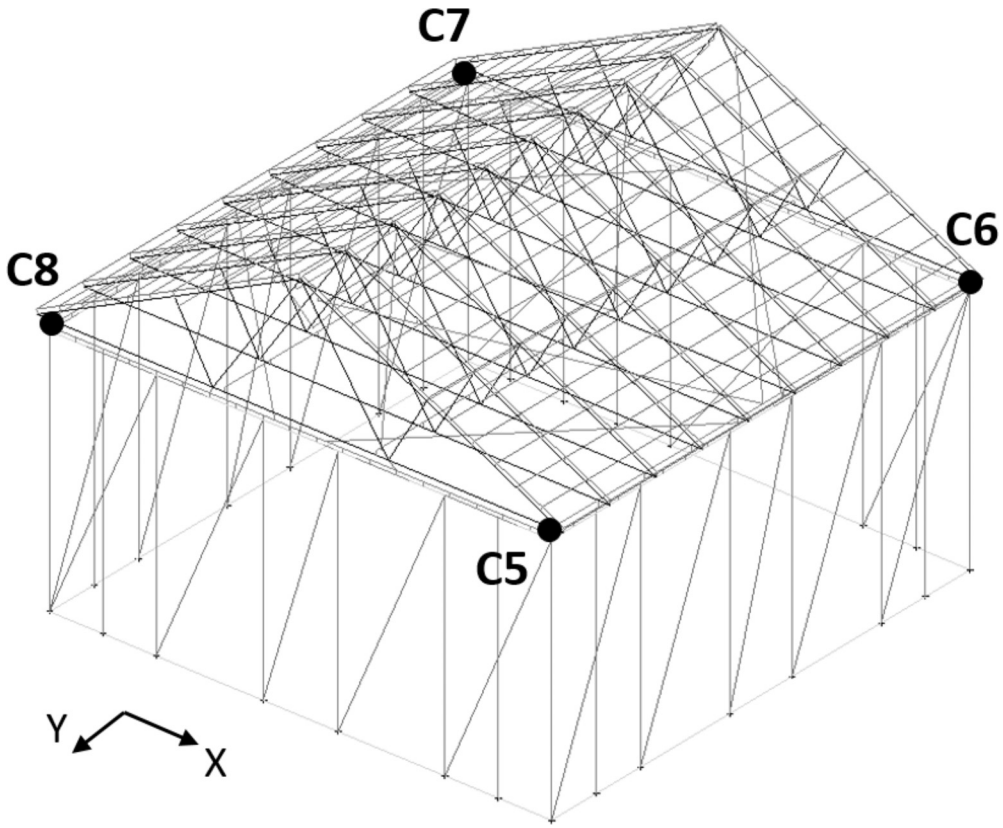

whether in shear or pull-out/compression; each behavior law is therefore assigned to the corresponding translational degree of freedom (DOF). This assumption does not hold for P2F joints, whose behavior is isotropic. The sill plate is assumed to be embedded since insignificant displacements were recorded during the tests. Each node of the top plate supports a nodal mass to account for the dead load imposed during the tests (Fig. 5*a*).

The input consists of the variability in the P2F nail joint. The propagation of uncertainty is initiated for shear walls associated with the N19 configuration (Table 1). An analysis of the experimental data from the five cyclic tests led to selecting a uniform probability law between 630 and 880 N for parameter F_1 (i.e., a 72 N standard deviation and a 9.6% coefficient of variation). A uniform probability law was chosen for three distinct reasons: (1) the number of test results on nails is limited (two monotonic tests and five cyclic tests); (2) the variability of test results is quite large; and (3) our aim here is not to accurately represent the joint strength distribution but instead to propagate uncertainty through the FE models, first at the scale of a single shear wall under static load and then under dynamic load. Moreover, the resulting CV of 9.6% is of the same order of magnitude as the average CV (12.5%), which was calculated over the 165 cyclic tests performed on P2F joints (Table 2). One hundred sets of uniformly distributed resistance F_1 of nail joints have been generated. These 100 representations of mechanical uncertainties of joints were then propagated through the shear wall FE models. Using the Monte-Carlo method, an average 8-mm maximum displacement was found at the top of the shear wall with a 2.5% CV.

3.3. Propagation of uncertainty through a 3D FE model of a house

The FE model of the house (Fig. 6) has been derived by using simplified FE models of shear walls. The FE model of the roof follows the same modeling principles as the refined models of shear walls (Boudaud et al. 2014). The shear walls have been modeled by means of four-node parallelogram macro-elements with just one translational DOF. Their shear response is described thanks to a hysteretic constitutive law similar to that developed for joints and calibrated to reproduce the results of the refined FE model calculations presented above. The FE model of the house has been built by assembling the simplified FE models of shear walls in conjunction with kinematic relations. The roof is attached to the simplified shear walls by spring-like elements that model the 3D bracket-type connectors. This deterministic FE model provides time-history displacements, which may be compared to the experimental measurements at each sensor location. The relative displacements at the top of the shear walls will be analyzed below. Figure 6 shows a perspective view with the two axes of acceleration. Figure 7*a* provides a top view of the house, the direction of the roof ridge and the position of the two doors, one of standard dimension (1.2 m wide) the other larger (1.96 m wide). Displacement measurements were available at each corner of the house. In the *X* direction, sensors C5 and C8 yielded, as expected, somewhat similar relative displacements (the same for C6 and C7). The peak displacements given in Fig. 7*a* are therefore the average values over two measurements. The numerical results are quite close to the experimental findings. Of note, the torsion is due to the slight asymmetry of the structure (due to a large door between C5 and C8). Figure 7*b* displays the time-history comparison of calculated and measured displacements at point C8; Figs. 7*c* and 7*d* show the same analysis for displacements in the *Y* direction (point C6).

The variability of shear walls is taken into account thanks to the parameter F_1 of macro-elements, which is considered to be the sole variable parameter. At the scale of the house, 3D bracket-type connectors and nail joints in the roof also constitute a source of uncertainty, which has been taken into account by establishing a

Fig. 7. Experimental and numerical comparison: (*a*) *X* - Average displacement at the top of the wall (mm); (*b*) *X* - Time-history comparison at C8 sensor; (*c*) *Y* - Average displacement at the top of the wall (mm); and (*d*) *Y* - Time-history comparison at C6 sensor.

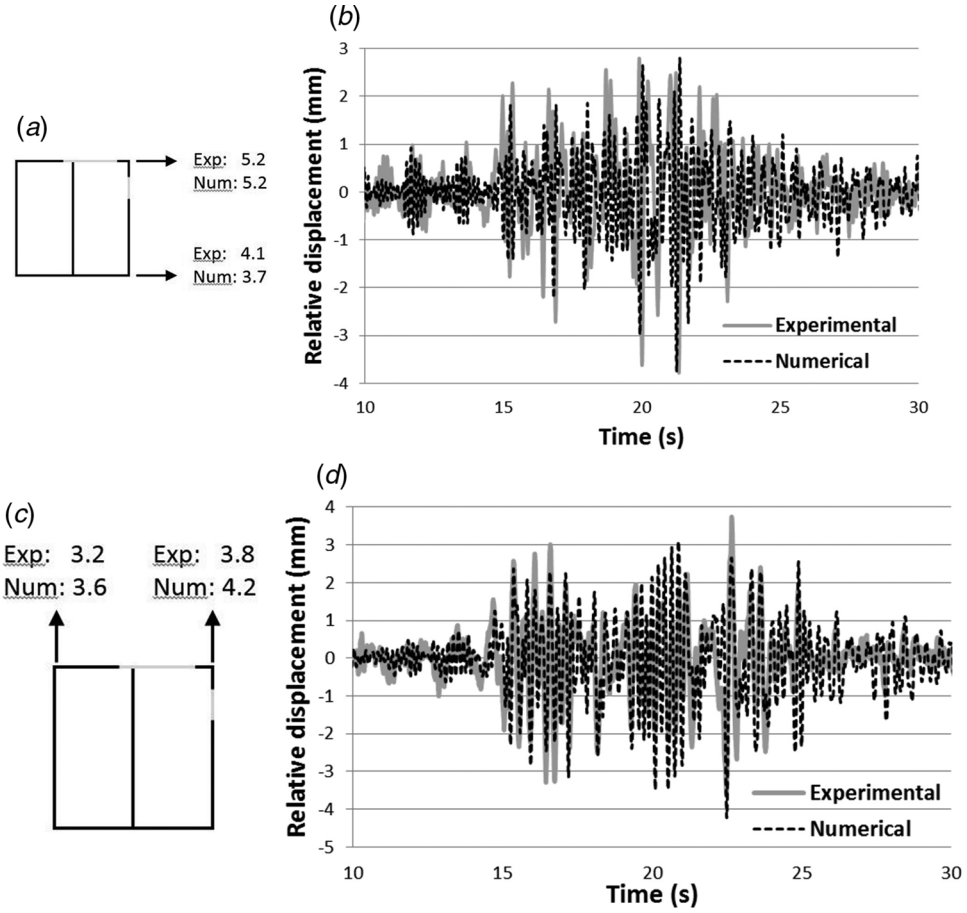

probabilistic law for their F_1 parameter. According to the test results listed in Table 5, a normal distribution law is introduced for F_1 based on a CV of 10%. For the roof nail connections, a normal distribution law has also been used. For the N1 configuration, the average F_1 equals 2250 N and the CV is 20%; for the N2 configuration, the average F_1 equals 2500 N and the CV is 7%. These 100 representations of mechanical uncertainties of joints have thus been propagated through the FE house model. Since this model requires over 15 h of computation time to be run, the Monte-Carlo method cannot be practically used. In this case, the stochastic collocation method (Baroth et al. 2007) has been introduced to approximate both the CV and cumulative distribution function (CDF) of displacement (Fig. 8). The CDF of displacement at value *x* is the probability that displacement takes a value less than or equal to *x*. Figure 8 shows very low probabilities of obtaining a maximum displacement less than 3.75 mm or more than 4.25 mm, with an average displacement around 4.1–4.2 mm (probability of 0.5). Regardless of the points analyzed (Fig. 7), CV values of less than 3% were found. This result demonstrates once again that while the variability of mechanical joints is relatively significant, its effect at the wall scale remains insignificant.

3.3.1. Discussion: Material versus load variability effects

The experimental and numerical displacement time-histories shown in Fig. 7 are quite similar. Figure 8 shows an example of the CDF of maximum displacements (at point C8, see Fig. 6); it can be observed that the experimental value (3.8 mm) is between the limits of the numerical distribution of displacements. Nevertheless, this distribution merely accounts for the variability in joint strength, although its variation domain would be larger if other

Fig. 8. CDF of the C8 displacement, *Y*-direction (mean: 4.2 mm, CV: 2.4%, experimental value: 3.8 mm).

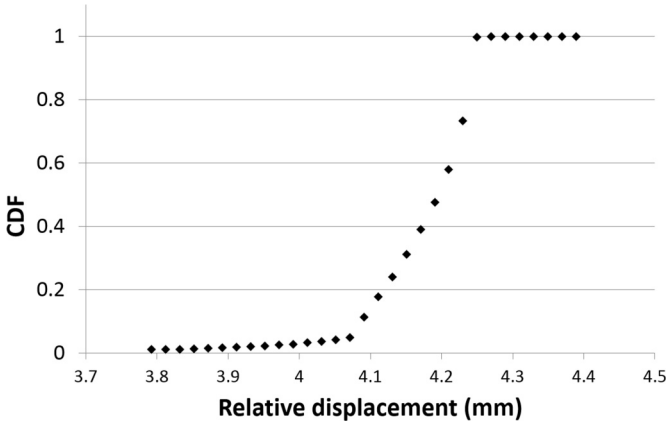

sources of variability were taken into account. More specifically, it is worth recalling that only one time-history accelerogram has been applied, and this accelerogram is not even representative of the seismic hazard. To further highlight this point, the same 2D FE shear wall model has been used with the seismic load being represented by a sufficient number of accelerograms to account for seismic loading variability. Moreover, an appropriate model of the input seismic action has been chosen. An earthquake event is characterized by a site-specific seismic hazard and earthquake motion records, whether historic (Bommer and Acevedo 2004;

Fig. 9. Influence of the number of accelerograms on the numerical convergence of means and standard deviations of: (*a*) PGA (m/s²); and (*b*) maximum wall displacements (mm).

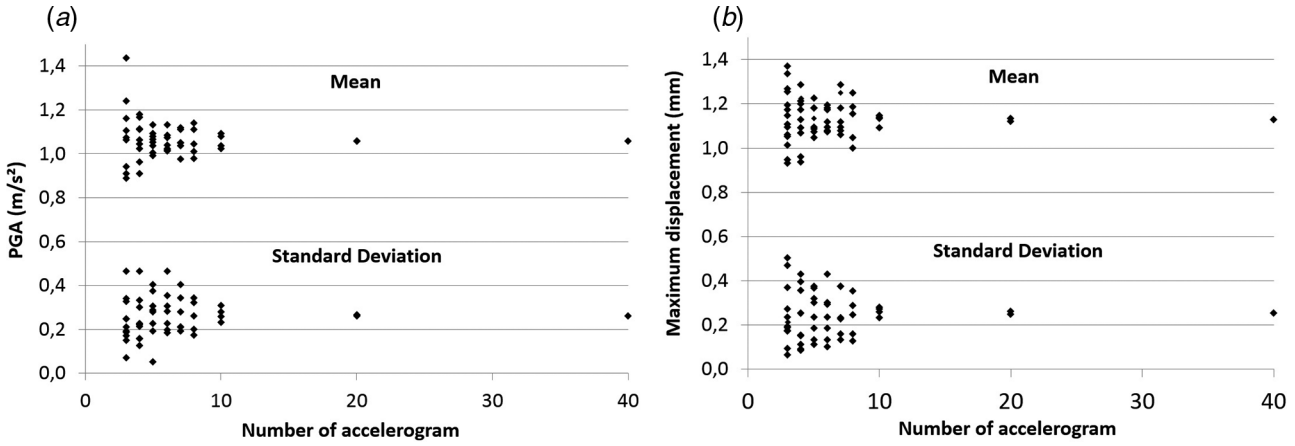

Hancock et al. 2008; Stefanou and Fragiadakis 2009) or artificial (Gasparini and Vanmarcke 1976; Pousse et al. 2006; Viallet and Humbert 2007; Zhang and Foschi 2004). Although several codes for designing earthquake-resistant buildings (Eurocode 8 - CEN 2004, NBCC 2005, ASCE 2005) suggest using just 3 (for the maximum value of the considered design parameter) or 7 (for the average value) accelerograms from the same scenario, Zhang and Foschi (2004) used 20 artificial ground motion accelerations in modeling peak ground acceleration as a lognormal random variable. These choices however were not specifically justified. Viallet and Humbert (2007) suggested a method for determining a conservative number of accelerograms based on statistical considerations. They applied a Student-Fisher estimator to predict the mean value of the population and observed the evolution of the quotient (mean of simulations/mean of population). Their study concluded that a minimum of 30 accelerograms is required to observe numerical convergence of the PGA, the strong-motion duration and the central frequency. In this study, 40 accelerograms have thus been generated in applying the model by Pousse et al. (2006) using a program developed based on the K-NET database (NRIESDP 2009). This method allows generating accelerograms based on common indicators in earthquake engineering, namely: peak ground acceleration (PGA), strong-motion duration, Arias intensity, and central frequency. For the sake of simplicity, only the PGA has been modeled arbitrarily using a Gaussian law. Figure 9*a* presents the numerical convergence of means and standard deviations of PGA for 3 to 40 accelerograms; this figure illustrates the major variability when using fewer than 20 accelerograms. The average PGA stands at around 0.11*g* (corresponding to zone 3 (out of 5) of the French seismic hazard map), while the standard deviation is near 0.025*g*, i.e., for a coefficient of variation equal to 22%. Figure 9*b* shows the numerical convergence of the means and standard deviations of the FE displacements of shear walls for 3 to 40 accelerograms. These results indicate that the CV of wall displacements is of the same order of magnitude (24.5%) as the input.

Table 6 summarizes the various results by providing the input and output CV values. For joints, the variable is maximum force, while it is PGA for the accelerograms. Outputs consist of relative displacements at the top of the walls.

Table 6. Input and output CV values.

Type	Input	CV (%)	2D shear wall	3D house
Material	Sheathing-to-framing nails	12	2.5	2.5–3
	Anti-buckling nails	20	—	
	Bracket-type joints	10	—	
Seismic load	Accelerogram	25	24.5	—

4. Conclusion

The first main feature of this paper pertains to quantifying the mechanical behavior variability of joints under both monotonic and cyclic loadings. Various types of joints and configurations have been evaluated during a total of more than 400 tests conducted. This extensive campaign has allowed quantifying their variability, which is significant, by displaying a joint strength CV value of between 10% and 20% depending on the connector type.

The second main feature concerns the propagation of uncertainty through an FE model of a shear wall and then another model of a timber-frame, single-story house. For this purpose, the data collected on sheathing-to-framing joints have been used as input in a refined FE shear wall model to study the propagation of uncertainty from the joints to the wall in a nonlinear transient calculation. The deterministic shear wall model had been contrasted with experimental results in previous papers (Humbert et al. 2014; Boudaud et al. 2014). Results here show that the variability of the maximum wall displacement is much smaller (CV = 2.5%) than that of the joints (CV = 12%). This same process has been carried out on the FE model of a 6 m ×6 m timber-frame house, leading to the finding that the variability in peak displacement during the dynamic motion (from 2.5% to 3%) is roughly the same as the shear wall variability (2.5%). When considering the good planar and elevation regularity of the studied structure, this result was to be expected. Nevertheless, this result has validated that an FE model could be developed for more complex cases (non-regular in plan and (or) elevation, multi-story buildings).

The third main feature is validation of the FE model for a single-story timber-frame house. The deterministic model predictions, based on a nonlinear dynamic calculation, have been compared with the results from a shaking table. Both numerical and experimental results are relatively similar, thus demonstrating the relevance of the model and its ability to study the propagation of uncertainty.

Lastly, the FE shear wall model has been used to perform the propagation of uncertainty due to the variability of seismic events. In all, 40 accelerograms were generated, leading to a PGA variability. Numerical results have shown that the variability in peak house displacement is the same as that obtained for the PGA of generated signals. Due to computational limitations, this calculation could not be conducted at the scale of the house. It is expected that the previous conclusion obtained for shear walls would apply to the house as well. Consequently, in the case of the

simple 6 m × 6 m one-story house studied in this paper, such results have confirmed that the effect of material variability is insignificant compared to the effect of seismic action variability. This key result still needs to be confirmed for more complex structures (i.e., with torsion effects or with several stories) and for other sources of uncertainties such as construction malpractice. The approach proposed herein has allowed quantifying the effects of uncertainties and could be used to justify the q factor introduced into the European seismic design code for buildings. This latter calculation can be achieved, for any accelerogram, by using the FE model to calculate the PGA leading to the limit of elasticity of the structure and the PGA corresponding to a failure limit. The ratio between these two PGA is a way of calculating the q factor. According to the results presented in this paper, the calculation of the q factor could take into account the variability of the seismic load considering that the effect of the material variability can be neglected.

Acknowledgements

The SISBAT research project was funded by the ANR (National Research Agency - through ANR-08-RISKNAT-008). The authors would like to express their gratitude for this support and thank the members of this project for their valuable contributions, especially Mrs. C. Faye (FCBA Technological Institute), Mr. P.E. Charbonnel, Mr. Chaudat (CEA) and their colleagues for the effort they provided in conducting the experimental campaign. Dr. J. Humbert, L. Davenne and Professor M. Yasumura were also instrumental in the successful completion of this project.

References

ASCE. 2005. ASCE 7-05, Minimum design loads for buildings and other structures. Including Supplement No. 1, Amercian Society of Civil Engineers, Reston, Va.

Baroth, J., Chauvière, C., Bressolette, P., and Fogli, M. 2007. An efficient SFE method using Lagrange Polynomials: application to nonlinear mechanical problems with uncertain parameters. Computer Methods in Applied Mechanics and Engineering, **196**: 4419–4429. doi:10.1016/j.cma.2007.04.017.

Bommer, J., and Acevedo, A.B. 2004. The use of real earthquake accelerograms as input to dynamic analysis. Journal of Earthquake Engineering, **8**(SI 1): 49–91. doi:10.1080/13632460409350521.

Boudaud, C., Hameury, S., Faye, C., and Daudeville, L. 2010. European seismic design of shear walls: experimental and numerical tests and observations. *In* 11th World Conference on Timber Engineering. WCTE 2010, Trentino, Italy.

Boudaud, C., Baroth, J., Hameury, S., and Daudeville, L. 2013. Multi-scale modelling of timber-frame structures under seismic loading. 12th International conference on computational plasticity. Complas XII, Barcelona, Spain.

Boudaud, C., Humbert, J., Baroth, J., Hameury, S., and Daudeville, L. 2014. Joints and wood shear walls modeling II: Experimental tests and FE models under seismic loading. Engineering Structures, **101**: 743–749. doi:10.1016/j.engstruct.2014.10.053.

Boudreault, F.A., Blais, C., and Rogers, C.A. 2007. Seismic force modification factors for light-gauge steel-frame – wood structural panel shear walls. Canadian Journal of Civil Engineering, **34**: 56–65. doi:10.1139/l06-097.

Ceccotti, A., and Karacabeyli, E. 2002. Validation of seismic design parameters for wood-frame shearwall systems. Canadian Journal of Civil Engineering, **29**: 484–498. doi:10.1139/l02-026.

CEN. 2004. Eurocode 8: Design of structures for earthquake resistance. Comité Européen de Normalisation, Brussels.

Charbonnel, P.-E., Baroth, J., Boudaud, C., and Daudeville, L. 2014. Experimental and numerical assessment of the seismic performance of a full-scale timber house. *In* 6th World Conference on Structure Control and Monitoring, WCSCM, Barcelona, Spain.

Dinehart, D.W., and Shenton, H.W., III. 1998. Comparison of static and dynamic response of timber shear walls. Journal of Structural Engineering, **124**(6): 686–695. doi:10.1061/(ASCE)0733-9445(1998)124:6(686).

Dujic, B., and Zarnic, R. 2004. Method for modeling dynamic response of timber frame building. 8th World Conference on Timber Engineering. WCTE 2004. Lahti, Finland.

EDF. 2014. Code_Aster. http://www.code-aster.org.

Filiatrault, A. 1990. Static and dynamic analysis of timber shear walls. Canadian Journal of Civil Engineering, **17**(4): 643–651. doi:10.1139/l90-073.

Filiatrault, A., Fischer, D., Folz, B., and Ugang, C. 2002. Experimental parametric study on the in-plane stiffness of wood diaphragms. Canadian Journal of Civil Engineering, **29**: 554–566. doi:10.1139/l02-036.

Foliente, G.C. 1997. Modeling and analysis of timber structures under seismic loads: State-of-the-art. *In* Earthquake performance and safety of timber structures. pp. 55–73. Forest products society meeting, Madison, USA.

Foliente, G.C. 2000. Reliability assessment of timber shear walls under earthquake loads. *In* 12th World Conference on Earthquake Engineering. 12WCEE 2000. Auckland, New-Zealand.

Fonseca, F., Rose, S., and Campbell, S. 2002. Nail, wood screw, and staple fastener connections. Consortium of Universities for Research in Earthquake Engineering.

Foschi, R.O. 1974. Load-slip characteristics of nails. Wood Science, **7**(1): 69–76.

Fulop, L., Ruff, A., Balint-Major, S., and Dubina, D. 2006. Seismic performance of timber shear walls sheathed with OSB panels. *In* International Workshop on Earthquake Engineering on Timber Structures. Coimbra, Portugal.

Gasparini, D.A., and Vanmarcke, E.H. 1976. Simulated earthquake motions compatible with prescribed response spectra. MIT civil engineering research report R76-4. Massachusetts Institute of Technology, Cambridge, MA, USA.

Germano, F., Metelli, G., and Giuriani, E. 2015. Experimental results on the role of sheathing-to-frame and base connections of a European timber framed shear wall. Construction and Building Materials, **80**: 315–328. doi:10.1016/j.conbuildmat.2015.01.076.

Hancock, J., Bommer, J., and Stafford, P.J. 2008. Numbers of scaled and matched accelerograms required for inelastic dynamic analyses. Earthquake Engineering and Structural Dynamics, **37**(14): 1585–1607. doi:10.1002/eqe.827.

He, M., Lam, F., and Foschi, R. 2001. Modeling the three-dimensional timber light-frame buildings. Journal of Structural Engineering, **127**(8); 901–913. doi:10.1061/(ASCE)0733-9445(2001)127:8(901).

Humbert, J., Baroth, J., Daudeville, L., Faye, C., Yasumura, M., and Davenne, L. 2009. SFE analysis of a timber frame undergoing a seismic load – Sensitivity analysis of a nail plate joint. *In* 10th International Conference on Structural Safety and Reliability (ICOSSAR). IASSAR, Osaka, Japan.

Humbert, J., Boudaud, C., Baroth, J., Hameury, S., and Daudeville, L. 2014. Joints and wood shear walls modelling I: Constitutive law, experimental tests and FE model under quasi-static loading. Engineering Structures, **65**: 52–61. doi:10.1016/j.engstruct.2014.01.047.

Lam, F., Filiatrault, A., Kawai, N., Nakajima, S., and Yamaguchi, N. 2002. Performance of timber buildings under seismic load. Part I: experimental studies. Progress in Structural Engineering and Materials, **4**(3): 276–285. doi:10.1002/pse.121.

Li, Y., and Ellingwood, B.R. 2007. Reliability of woodframe residential construction subjected to earthquakes. Structural Safety, **29**: 294–307. doi:10.1016/j.strusafe.2006.07.012.

NBCC (National Building Code of Canada). 2005. 12th ed. National Research Council Canada, Ottawa, Ont.

NRIESDP (National Research Institute for Earth Science and Disaster Prevention). K-NET and KiK-net networks. 2009. http://www.kyoshin.bosai.go.jp.

Pei, S., and van de Lindt, J.W. 2010. Influence of structural properties and hazard level on seismic loss estimation for light-frame wood structures. Engineering Structures, **32**: 2183–2191. doi:10.1016/j.engstruct.2010.03.021.

Pei, S., van de Lindt, J.W., Ni, C., and Pryor, S.E. 2010. Experimental seismic behaviour of a five-storey double-midply wood shear wall in a full scale building. Canadian Journal of Civil Engineering, **37**(9): 1261–1269. doi:10.1139/L10-058.

Pousse, G., Bonilla, L.F., Cotton, F., and Margerin, L. 2006. Nonstationary stochastic simulation of strong ground motion time histories including natural variability: Application to the K-Net Japanese database. Bulletin of the Seismological Society of America, **96**(6): 2103–2117. doi:10.1785/0120050134.

Riahi, H., Chateauneuf, A., Bressolette, P., and Fournely, E. 2013. Reliability analysis of nonlinear timber roofs under seismic loading. *In* 11th International Conference on Structural Safety and Reliability, ICOSSAR. New York, USA.

Richard, N., Daudeville, L., Prion, H., and Lam, F. 2002. Timber shear walls with large openings: experimental and numerical prediction of the structural behaviour. Canadian Journal of Civil Engineering, **29**(5): 713–724. doi:10.1139/l02-050.

Rosowsky, D.V. 2002. Reliability-based seismic design of wood shear walls. Journal of Structural Engineering, **128**(11): 1439–1453. doi:10.1061/(ASCE)0733-9445(2002)128:11(1439).

Sartori, T., and Tomasi, R. 2013. Experimental investigation on sheathing-to-framing connections in wood shear walls. Engineering Structures, **56**: 2197–2205. doi:10.1016/j.engstruct.2013.08.039.

Shenton, H.W., III, Dinehard, D.W., and Elliott, T.E. 1997. Stiffness and energy degradation of wood frame shear walls. Canadian Journal of Civil Engineering, **25**: 412–423. doi:10.1139/l97-108.

Stefanou, G., and Fragiadakis, M. 2009. Nonlinear dynamic analysis of frames with stochastic non-Gaussian material properties. Engineering Structures, **31**(8): 1841–1850. doi:10.1016/j.engstruct.2009.02.020.

Tamaris. 2015. http://www-tamaris.cea.fr/index_en.php.

Verdret, Y., Faye, C., Elachachi, S.M., Le Magorou, L., and Garcia, P. 2015. Experimental investigation on stapled and nailed connections in light timber frame walls. Construction and Building Materials, **91**: 260–273. doi:10.1016/j.conbuildmat.2015.05.052.

Viallet, E., and Humbert, N. 2007. Considerations on the use of natural and synthetic time histories for seismic transient non-linear analyses of structures and variability assessment. Transactions, SMiRT19, Toronto.

White, M.W., and Dolan, J.D. 1995. Nonlinear shear-wall analysis. Journal of Structural Engineering, **121**(11): 1629–1635. doi:10.1061/(ASCE)0733-9445(1995)121:11(1629).

Xu, J., and Dolan, J.D. 2009. Development of a wood-frame shear wall model in Abaqus. Journal of Structural Engineering, **135**(8): 977–984. doi:10.1061/(ASCE)ST.1943-541X.0000031.

Yin, Y.J., and Li, Y. 2010. Seismic collapse risk of light-frame wood construction considering aleatoric and epistemic uncertainties. Structural Safety, **32**: 250–261. doi:10.1016/j.strusafe.2010.03.012.

Zhang, J., and Foschi, R.O. 2004. Performance-based design and seismic reliability analysis using designed experiments and neural networks. Probabilistic Engineering Mechanics, **19**: 259–267. doi:10.1016/j.probengmech.2004.02.009.